



Crystal structure, morphotropic phase transition and luminescence in the new cyclosilicates $\text{Sr}_3\text{R}_2(\text{Si}_3\text{O}_9)_2$, R=Y, Eu–Lu

Alexander P. Tyutyunnik, Ivan I. Leonidov*, Ludmila L. Surat, Ivan F. Berger, Vladimir G. Zubkov

Institute of Solid State Chemistry, UB RAS, 620990 Ekaterinburg, Russian Federation

ARTICLE INFO

Article history:

Received 18 July 2012

Received in revised form

5 September 2012

Accepted 9 September 2012

Available online 16 September 2012

Keywords:

Rietveld refinement

X-ray diffraction

Silicates

Luminescence

ABSTRACT

A new series of promising luminescent materials, cyclosilicates $\text{Sr}_3\text{R}_2(\text{Si}_3\text{O}_9)_2$, R=Y, Eu–Lu, has been synthesized via a solid-state reaction. X-ray and neutron powder diffraction studies show that these oxides crystallize in the monoclinic crystal system (S.G. $C2/c$, $Z=4$) and have a morphotropic phase transition between Er and Tm compounds followed by a step-like change of the unit cell constants. Isolated $[\text{Si}_3\text{O}_9]$ rings located in layers are basic building units and stack with Sr/R layers along the $[1\ 0\ \bar{1}]$ direction. The rare earth atoms are distributed among three independent Sr/R sites coordinated by 8, 7 and 6 oxygen atoms, and the Sr-R populations change from mixed to 0.5/0.5 over site (1) and full occupation of sites (2) and (3) by Sr and R, respectively, at the transition. Changes of the conformation and mutual arrangement of $[\text{Si}_3\text{O}_9]$ rings, as well as exchange of oxygen atoms from the first and the second coordination sphere of two Sr/R sites also feature the phase transition. Luminescence in $\text{Sr}_3\text{Y}_2(\text{Si}_3\text{O}_9)_2:\text{Eu}^{3+}$ under ultraviolet (UV) excitation has been discussed.

© 2012 Elsevier Inc. All rights reserved.

1. Introduction

In the past decades, phosphors with ultraviolet (UV) excitation for plasma display panels (PDPs), Hg-free lamps and LCD backlight applications and their fundamental research have received much attention [1–4]. Many reports on compounds in $\text{CaO}-\text{Y}_2\text{O}_3-\text{SiO}_2$ system have been published because it is a basic and important system for inorganic luminescent materials with high thermal and chemical stability [5–11]. Crystal structures of quaternary compounds $\text{Ca}_3\text{Y}_2(\text{SiO}_4)_3$ [12,13], $\text{Ca}_2\text{Y}_2\text{Si}_2\text{O}_9$ [14], $\text{Ca}_2\text{Y}_8(\text{SiO}_4)_6\text{O}_2$ [15,16], $\text{Ca}_3\text{Y}_6(\text{SiO}_4)_6$ [16], $\text{Ca}_4\text{Y}_6(\text{SiO}_4)_6\text{O}$ [16] and $\text{Ca}_3\text{Y}_2(\text{Si}_3\text{O}_9)_2$ [17,18] comprise either discrete SiO_4 tetrahedra ($\text{Ca}_3\text{Y}_2(\text{SiO}_4)_3$, $\text{Ca}_2\text{Y}_8(\text{SiO}_4)_6\text{O}_2$), or Si_2O_7 pyrogroups ($\text{Ca}_2\text{Y}_2\text{Si}_2\text{O}_9$), or $[\text{Si}_3\text{O}_9]$ rings ($\text{Ca}_3\text{Y}_2(\text{Si}_3\text{O}_9)_2$) [19]. Luminescence properties of $\text{Ca}_3\text{Y}_2(\text{SiO}_4)_3$, $\text{Ca}_2\text{Y}_2\text{Si}_2\text{O}_9$, $\text{Ca}_2\text{Y}_8(\text{SiO}_4)_6\text{O}_2$, and $\text{Ca}_4\text{Y}_6(\text{SiO}_4)_6\text{O}$ doped with lanthanide ions have been discussed in numerous previous papers [20–35]. The energy transfer $\text{Ce}^{3+}\rightarrow\text{Tb}^{3+}$ in $\text{Ca}_3\text{Y}_2(\text{Si}_3\text{O}_9)_2:\text{Ce}^{3+},\text{Tb}^{3+}$ and room temperature and 10 K luminescence in $\text{Ca}_3\text{Y}_2(\text{Si}_3\text{O}_9)_2:\text{Tb}^{3+}$ under VUV-UV synchrotron radiation excitation have been reported by two research groups [36,37].

Most of quaternary phases in the $\text{R}_2\text{O}_3-\text{SrO}-\text{SiO}_2$ system (R =rare earth ion) have an apatite-type structure [38–43]. Another crystal structure of the mixed-framework trisilicate $\text{Sr}_2\text{Y}_2\text{Si}_3\text{O}_{10}$ contains slightly curved Si_3O_{10} and Y_2O_{11} structural units [44]. There are only a few modifications of $\text{Sr}_3(\text{Si}_3\text{O}_9)$ among cyclosilicates in this system with $[\text{Si}_3\text{O}_9]$ rings located in layers alternating

with strontium cations layers [8,45–47] and the high-pressure δ' -phase $\text{Sr}_4(\text{Si}_4\text{O}_{12})$ with tetra-cycles $[\text{Si}_4\text{O}_{12}]$ [8]. The hexagonal $\text{La}_3\text{F}_3[\text{Si}_3\text{O}_9]$, closely related to this system, has ideal tri-cycles [48], $\text{Sr}_8(\text{Si}_4\text{O}_{12})\text{Cl}_8$ and $\text{Eu}_2\text{Cl}_2(\text{SiO}_3)$ have tetra-cycles [49,50] and $\text{Na}_2\text{Sr}(\text{Si}_2\text{O}_6)$ has hexa-cycles [51] in the crystal structure. $\text{Ca}_3\text{Y}_2(\text{Si}_3\text{O}_9)_2$ derived from a wadeite α - CaSiO_3 (pseudowollastonite, a high-temperature polymorph of CaSiO_3 [52]) has been studied in detail by Yamane et al. [17] and its structure has been compared with structures of closely related silicates. This compound crystallizes in the space group $C2/c$ ($Z=4$). Ca and Y atoms are in eight-, seven- and sixfold coordination sites between the layers of $[\text{Si}_3\text{O}_9]$ rings. The average Si-Si distances 3.035 Å were reported to be consistent with the non-bonding distance $2R=3.06$ Å for regular SiO_4 tetrahedra [53], which O'Keeffe and Hyde used to explain the rarity of ternary SiO_4 rings, i.e. $[\text{Si}_3\text{O}_9]$, in silicate structures and the anomalously long strained Si-O bonds observed in the 3-rings. In this paper, we report crystal structure, morphotropic phase transition (MPT [54]) in the new group of cyclosilicates $\text{Sr}_3\text{R}_2(\text{Si}_3\text{O}_9)_2$, R=Y, Eu–Lu, and visible luminescence in $\text{Sr}_3\text{Y}_2(\text{Si}_3\text{O}_9)_2:\text{Eu}^{3+}$ under UV excitation.

2. Materials and methods

A series of silicates $\text{Sr}_3\text{R}_2(\text{Si}_3\text{O}_9)_2$, R=Y, Eu, Gd, Tb, Dy, Ho, Er, Tm, Yb, Lu, was prepared via a solid-state reaction route at ambient pressure from stoichiometric mixtures of SrCO_3 (99.95%), R_2O_3 (99.98%) and amorphous SiO_2 (99.995%). The samples were pressed into pellets, placed in alumina boats and annealed at $T=950$ °C for 1–2 h, for SrCO_3 decarbonization to SrO ,

* Corresponding author.

E-mail address: ivanleonidov@ihim.uran.ru (I.I. Leonidov).

and then at $T=1300\text{ }^{\circ}\text{C}$ for 150–200 h in air with intermediate regrinding in an agate mortar, and cooled down with the furnace. Terbium silicate was synthesized in the neutral atmosphere (Ar). The homogeneous solid solution $\text{Sr}_3\text{Y}_{2-x}\text{Eu}_x(\text{Si}_3\text{O}_9)_2$, $x=0.25\text{--}2$, was prepared from stoichiometric mixtures of $\text{Sr}_3\text{Y}_2(\text{Si}_3\text{O}_9)_2$ and $\text{Sr}_3\text{Eu}_2(\text{Si}_3\text{O}_9)_2$ samples by the same thermal processing.

The single-phase character of the final products was checked by X-ray powder diffraction. All X-ray powder diffraction (XRD) patterns were collected on a STADI-P automated diffractometer (STOE) equipped with a linear mini-PSD detector using $\text{Cu K}\alpha_1$ radiation in the 2θ range from 5° to 120° with a step of 0.02° . Polycrystalline silicon ($a=5.43075(5)\text{ \AA}$) was used as an external standard. Possible impurity phases were checked by comparing their XRD patterns with those in the PDF2 database (Powder diffraction file, ICDD, release 2009). Since scattering powers of Sr and Y in XRD experiments are very close, the neutron diffraction measurements of $\text{Sr}_3\text{Y}_2(\text{Si}_3\text{O}_9)_2$ have been carried out at room temperature on a D7A setup of the IVV 2M reactor (Zarechny, Russia) in the 2θ range from 10° to 125° with a 0.05° step and neutron wavelength $\lambda=1.5275\text{ \AA}$. The crystal structure refinement of $\text{Sr}_3\text{R}_2(\text{Si}_3\text{O}_9)_2$, R=Y, Eu–Lu, was carried out with the GSAS program suite using XRD data; in case of $\text{Sr}_3\text{Y}_2(\text{Si}_3\text{O}_9)_2$ both X-ray and neutron diffraction data were used simultaneously [55]. The peak profiles were fitted with a pseudo-Voigt function, $I(2\theta)=x*L(2\theta)+(1-x)*G(2\theta)$ (where L and G are the Lorentzian and Gaussian part, respectively). The angular dependence of the peak width was described by the relation $(FWHM)^2=Utg^2\theta+Vtg\theta+W$, where FWHM is the full line width at half maximum. The background level was described by a combination of 36-order Chebyshev polynomials. The absorption correction function for a flat plate sample in transmission geometry was applied [55].

The room temperature photoluminescence (PL) and photoluminescence excitation (PLE) spectra were recorded on a Varian Cary Eclipse fluorescence spectrophotometer coupled to a personal computer with Varian software and supplied with a 75 kW Xenon lamp as excitation source (pulse length $\tau=2\text{ }\mu\text{s}$, pulse frequency $v=80\text{ Hz}$, wavelength resolution 0.5 nm; PMT Hamamatsu R928).

3. Results and discussion

3.1. Structural analysis

The XRD patterns of $\text{Sr}_3\text{R}_2(\text{Si}_3\text{O}_9)_2$, R=Y, Eu–Lu, can be indexed with monoclinic unit cells $C2/c$ (S.G. No. 15, $Z=4$), with the

constants following the linear dependence upon the crystal radius [56] of rare earth ions until MPT between Er and Tm compounds accompanied by a step-like decrease in a , c and V and an increase in b and β (Table 1, Fig. 2). Since the nominal composition of the synthesized $\text{Sr}_3\text{R}_2(\text{Si}_3\text{O}_9)_2$ compounds corresponds to the formula of $\text{Ca}_3\text{Y}_2(\text{Si}_3\text{O}_9)_2$, the latter was used as a starting model for the crystal structure refinement [17]. Structural data, atomic coordinates and isotropic thermal parameters are listed in Tables 1 and 2. All data for $\text{Sr}_3\text{Y}_2(\text{Si}_3\text{O}_9)_2$ are placed among those for rare earth silicates according to crystal radius. The mass fractions of impurity phases used in the full-profile fitting are shown as m. % (Table 1). The fractions of strontium in the $\text{Sr}(2)/\text{R}(2)$ sites for Tm, Yb and Lu were found to exceed 1.0 less than in three standard deviations and were fixed to 1.0, the fractions in the $\text{Sr}(1)/\text{R}(1)$ and $\text{Sr}(3)/\text{R}(3)$ sites were constrained to keep the overall composition $\text{Sr}_3\text{R}_2(\text{Si}_3\text{O}_9)_2$. Fig. 1(a, b) displays experimental, calculated and difference XRD patterns for the Er and Tm samples, respectively. The selected interatomic distances, bond angles and the specific distances in $\text{Sr}_3\text{R}_2(\text{Si}_3\text{O}_9)_2$, R=Y, Eu–Lu, are listed in Tables 3 and 4. The difference in neutron cross-section for Sr and Y, 0.702 and 0.775,

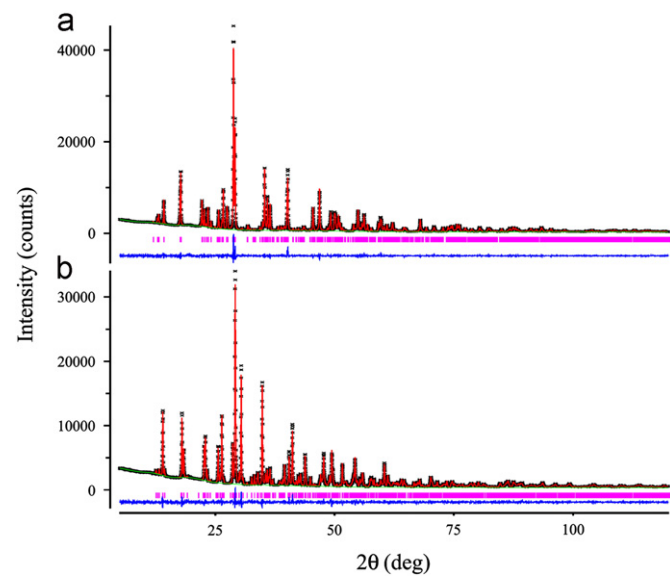


Fig. 1. Observed (crosses), calculated (solid line) and difference (bottom) XRD patterns for $\text{Sr}_3\text{Er}_2(\text{Si}_3\text{O}_9)_2$ (a) and $\text{Sr}_3\text{Tm}_2(\text{Si}_3\text{O}_9)_2$ (b).

Table 1
Structural data for $\text{Sr}_3\text{R}_2(\text{Si}_3\text{O}_9)_2$, R=Y, Eu–Lu.

Parameter	Eu	Gd	Tb	Dy	Y	Ho	Er	Tm	Yb	Lu
Crystal system	Monoclinic									
Space group	$C2/c$ (No. 15)									
Cell constants										
$a, \text{\AA}$	13.6036(9)	13.5863(9)	13.5492(9)	13.5396(9)	13.5220(9)	13.5206(9)	13.5027(9)	13.3937(9)	13.3924(9)	13.3777(9)
$b, \text{\AA}$	8.0219(7)	8.0130(7)	8.0005(7)	7.9894(7)	7.9750(7)	7.9798(7)	7.9741(7)	8.2608(7)	8.2542(7)	8.2518(7)
$c, \text{\AA}$	14.9987(9)	14.9630(9)	14.8909(9)	14.8601(9)	14.8353(9)	14.8240(9)	14.7791(9)	13.7065(9)	13.6825(9)	13.6627(9)
β, deg	89.526(6)	89.698(6)	89.837(6)	90.004(6)	90.157(6)	90.161(6)	90.297(6)	93.328(6)	93.394(6)	93.477(6)
$V, \text{\AA}^3$	1636.7	1629.0	1614.2	1607.5	1599.8	1599.4	1591.3	1514.0	1509.9	1505.4
Z	4	4	4	4	4	4	4	4	4	4
$D_{\text{calcd}}, \text{g} \cdot \text{cm}^{-3}$	4.151	4.214	4.260	4.311	3.722	4.356	4.401	4.637	4.687	4.717
m.% SrSiO_3	0.0	1.0	0.0	0.5	0.0	0.0	0.8	0.0	0.0	0.0
m.% $\text{Sr}_2\text{R}_8\text{O}_2(\text{SiO}_4)_6$	2.9	1.1	1.5	0.0	0.0	0.8	0.5	0.0	0.0	0.0
R_{wp}	1.55	1.32	2.12	1.97	3.92	4.43	5.06	4.83	4.59	4.71
R_p	1.18	0.99	1.62	1.49	3.34	3.37	3.89	3.60	3.35	3.53
$R(F^2) (\%)$	3.85	3.74	4.95	3.67	3.29	3.15	2.78	2.71	2.48	2.43
χ^2	1.672	2.026	1.911	1.810	3.775	2.776	3.323	3.195	5.378	3.125

Note: For neutron data of $\text{Sr}_3\text{Y}_2(\text{Si}_3\text{O}_9)_2$: $R_{\text{wp}}=2.21\%$, $R_p=1.75\%$, $R(F^2)=4.44\%$.

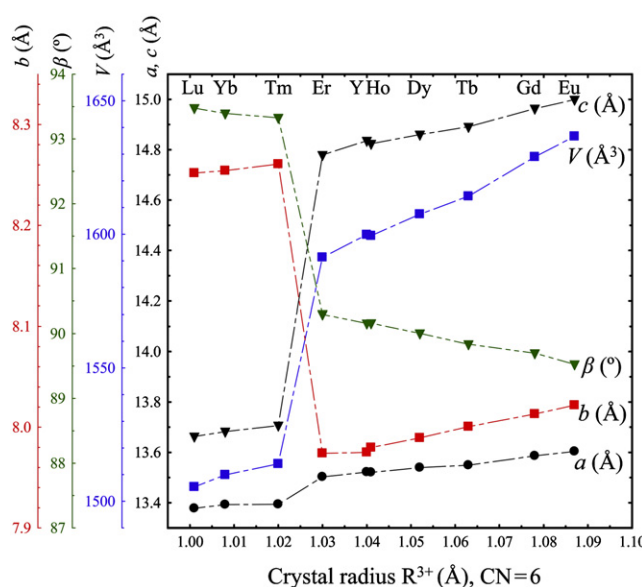


Fig. 2. Unit cell constants for $\text{Sr}_3\text{R}_2(\text{Si}_3\text{O}_9)_2$, $\text{R}=\text{Y}$, Eu-Lu , vs. the rare earth ion crystal radius in sixfold coordination [56] chosen as the site occupied mainly by rare earths.

Table 2

Refined atomic coordinates and isotropic thermal displacement parameters $U_{\text{iso}}^*(100)$ (\AA^2) for $\text{Sr}_3\text{R}_2(\text{Si}_3\text{O}_9)_2$, $\text{R}=\text{Y}$, Eu-Lu .

Parameter	R										
		Eu	Gd	Tb	Dy	Y	Ho	Er	Tm	Yb	Lu
$\text{Sr}(1)/\text{R}(1)$											
x/a	0.1599(2)	0.1597(3)	0.1621(3)	0.1618(4)	0.1607(2)	0.1611(2)	0.1617(2)	0.1659(1)	0.1658(1)	0.1657(2)	
y/b	0.1240(9)	0.1239(9)	0.1223(11)	0.1231(11)	0.1207(6)	0.1210(7)	0.1216(6)	0.1231(3)	0.1233(3)	0.1236(3)	
z/c	0.4122(2)	0.4119(2)	0.4123(3)	0.4112(3)	0.4127(2)	0.4114(2)	0.4123(2)	0.4077(1)	0.4082(1)	0.4088(1)	
U^*100	2.7(1)	2.4(2)	2.3(3)	3.0(2)	0.91(9)	2.9(1)	3.1(1)	2.7(1)	2.5(1)	2.9(1)	
Fraction	0.698/0.302(6)	0.66/0.34(1)	0.67/0.33(1)	0.66/0.34(1)	0.63/0.37(1)	0.63/0.37(1)	0.64/0.36(1)	0.493/0.507(4)	0.494/0.506(3)	0.488/0.512(4)	
$\text{Sr}(2)/\text{R}(2)$											
x/a	0.3402(3)	0.3389(3)	0.3355(4)	0.3402(4)	0.3410(2)	0.3406(2)	0.3413(2)	0.3479(1)	0.3479(1)	0.3480(2)	
y/b	0.1321(9)	0.1298(10)	0.1238(11)	0.1293(12)	0.1266(6)	0.1277(7)	0.1269(6)	0.1298(4)	0.1300(4)	0.1305(4)	
z/c	0.0784(2)	0.0794(3)	0.0800(4)	0.0772(3)	0.0785(2)	0.0768(2)	0.0770(2)	0.0459(1)	0.0470(1)	0.0478(1)	
U^*100	3.1(1)	3.0(2)	3.2(2)	3.8(2)	1.24(8)	3.0(1)	2.9(1)	3.1(1)	2.9(1)	3.2(1)	
Fraction	0.699/0.301(6)	0.71/0.29(1)	0.71/0.29(1)	0.73/0.27(1)	0.74/0.26(1)	0.74/0.26(1)	0.75/0.25(1)	1.0/0.0	1.0/0.0	1.0/0.0	
$\text{Sr}(3)/\text{R}(3)$											
x/a	0	0	0	0	0	0	0	0	0	0	
y/b	0.3798(6)	0.3783(7)	0.3754(9)	0.3788(8)	0.3773(6)	0.3766(6)	0.3758(5)	0.3738(3)	0.3726(3)	0.3711(3)	
z/c	1/4	1/4	1/4	1/4	1/4	1/4	1/4	1/4	1/4	1/4	
U^*100	2.5(2)	2.6(2)	4.6(3)	2.9(2)	2.7(1)	3.1(1)	2.9(1)	2.7(1)	2.3(1)	2.7(1)	
Fraction	0.21/0.79(1)	0.26/0.74(2)	0.26/0.74(2)	0.24/0.76(2)	0.26/0.74(2)	0.26/0.74(2)	0.21/0.79(2)	0.014/0.986(8)	0.012/0.988(7)	0.024/0.976(8)	
$\text{Si}(1)$											
x/a	0.0980(8)	0.0961(9)	0.1007(10)	0.096(1)	0.0985(5)	0.0954(7)	0.0973(6)	0.0875(5)	0.0879(4)	0.0874(5)	
y/b	0.065(1)	0.068(2)	0.075(2)	0.059(2)	0.0657(8)	0.063(1)	0.066(1)	0.0405(7)	0.0401(7)	0.0372(8)	
z/c	0.1097(8)	0.108(1)	0.113(1)	0.107(1)	0.1099(5)	0.1069(7)	0.1095(7)	0.1251(5)	0.1256(5)	0.1240(6)	
U^*100	2.3(4)	4.2(4)	2.1(5)	3.9(5)	1.1(2)	3.0(3)	3.5(3)	2.8(2)	2.7(2)	3.2(2)	
$\text{Si}(2)$											
x/a	0.2720(6)	0.2733(7)	0.2711(10)	0.2710(7)	0.2716(4)	0.2727(4)	0.2704(4)	0.2651(4)	0.2647(4)	0.2640(5)	
y/b	0.370(3)	0.372(4)	0.390(4)	0.371(4)	0.370(2)	0.377(2)	0.371(2)	0.368(2)	0.365(1)	0.365(2)	
z/c	0.2681(7)	0.2654(9)	0.262(1)	0.266(1)	0.2611(5)	0.2632(5)	0.2632(6)	0.2470(4)	0.2469(4)	0.2468(4)	
U^*100	3.8(4)	4.3(4)	5.3(7)	3.5(4)	3.0(2)	3.3(2)	3.3(2)	2.4(2)	2.1(2)	2.5(2)	
$\text{Si}(3)$											
x/a	0.4056(9)	0.4057(9)	0.411(1)	0.403(1)	0.4062(6)	0.4044(6)	0.4061(6)	0.4079(4)	0.4088(4)	0.4093(5)	
y/b	0.181(2)	0.180(2)	0.179(2)	0.181(2)	0.1787(9)	0.181(1)	0.183(1)	0.1872(7)	0.1869(6)	0.1850(7)	
z/c	0.4039(9)	0.400(1)	0.399(1)	0.399(1)	0.3969(6)	0.3941(7)	0.3946(6)	0.3823(5)	0.3819(5)	0.3803(5)	
U^*100	4.6(5)	3.8(4)	3.6(6)	4.5(6)	2.6(3)	3.0(3)	3.3(3)	1.7(2)	1.7(2)	2.0(2)	
O(1)											
x/a	0.010(2)	0.017(2)	0.017(3)	0.006(3)	0.006(1)	0.007(2)	0.002(2)	0.006(1)	0.005(1)	0.007(1)	
y/b	0.177(3)	0.183(3)	0.1826(32)	0.177(3)	0.177(1)	0.181(2)	0.173(2)	0.167(2)	0.163(2)	0.164(2)	
z/c	0.133(1)	0.137(2)	0.144(2)	0.135(2)	0.1366(7)	0.137(1)	0.135(1)	0.135(1)	0.134(1)	0.136(1)	
U^*100	3.5(9)	4.2(9)	3.5(3)	4.9(9)	3.4(4)	2.5(7)	5.2(7)	5.0(6)	5.8(6)	5.1(6)	
O(2)											
x/a	0.0568(9)	0.059(1)	0.059(1)	0.053(1)	0.0529(5)	0.0537(7)	0.0520(9)	0.0322(8)	0.0327(7)	0.0334(8)	
y/b	0.111(3)	0.115(4)	0.084(2)	0.125(4)	0.130(2)	0.125(3)	0.127(3)	0.132(2)	0.133(2)	0.139(2)	
z/c	0.578(1)	0.581(1)	0.595(2)	0.585(2)	0.5832(6)	0.5850(8)	0.5833(9)	0.6108(8)	0.6130(7)	0.6158(8)	

did not result in accurate and stable determination of the Sr/Y site populations, and the corresponding values of the Ho compound were used in the final refinement. Fig. 3 illustrates the crystal structures of the title cyclosilicates before and after MPT. At first sight, they show no considerable differences. In all cases the isolated $[\text{Si}_3\text{O}_9]$ rings located in layers are the basic building units and stack with Sr/R layers along the $[1\ 0\ \bar{1}]$ direction. The cyclic anion formed by three corner-shared tetrahedra SiO_4 demonstrates the following conformations: (a) sufficiently close to ideal configuration before transition (Y, Eu-Er), where bridging oxygen atoms are in the plane of the ring, passing through three silicon atoms, and O-O edges formed by the terminal oxygen atoms are normal to this plane, and (b) after the transition (Tm-Lu), where the bridging oxygen atoms are shifted below the plane of the ring and all tetrahedral apices are pointed up (Fig. 4). The former conformation and Si···Si distances about 3.03–3.08 Å (Table 3) are consistent with the non-bonding distance $2R(\text{Si})=3.06$ Å for regular SiO_4 tetrahedra [53] found in $\text{Ca}_3\text{Y}_2(\text{Si}_3\text{O}_9)_2$ [17] and $\text{Sr}_3(\text{Si}_3\text{O}_9)$ [45–47]. The latter conformation resulting in a significant shortening of the Si···Si distances to 2.94–2.95 Å, which are well below $2R(\text{Si})$, has been also reported for the high-pressure polymorph of NaYSi_2O_6 [57] and $(\text{Ca}_{1.3}\text{Sr}_{1.7})(\text{Si}_3\text{O}_9)$ [58]. Similar to the formalism given by Kahlenberg et al. [57], the arrangement within a single layer of the rings in $\text{Sr}_3\text{R}_2(\text{Si}_3\text{O}_9)_2$ can

Table 2 (continued)

Parameter	R									
	Eu	Gd	Tb	Dy	Y	Ho	Er	Tm	Yb	Lu
U^*100 O(3)	1.7(5)	3.9(8)	3.5(3)	4.0(6)	3.0(2)	2.6(4)	4.4(5)	3.0(4)	2.7(4)	2.7(4)
x/a	0.159(1)	0.161(2)	0.164(2)	0.154(2)	0.1577(5)	0.155(1)	0.153(1)	0.1603(9)	0.1603(8)	0.1582(9)
y/b	0.373(4)	0.382(5)	0.401(6)	0.369(5)	0.379(1)	0.382(3)	0.376(3)	0.365(2)	0.365(2)	0.368(2)
z/c	0.300(1)	0.299(1)	0.297(2)	0.298(1)	0.3015(5)	0.3003(7)	0.3009(8)	0.3057(9)	0.3072(8)	0.307(1)
U^*100 O(4)	1.6(6)	1.6(8)	3.5(3)	2.0(9)	1.5(2)	1.1(4)	2.0(4)	1.6(3)	1.4(3)	1.9(4)
x/a	0.170(2)	0.173(2)	0.162(2)	0.157(2)	0.1599(7)	0.158(1)	0.159(1)	0.1588(9)	0.1571(9)	0.158(1)
y/b	0.097(3)	0.099(3)	0.101(5)	0.095(4)	0.102(1)	0.103(3)	0.099(2)	0.072(2)	0.074(2)	0.074(2)
z/c	0.022(1)	0.019(1)	0.010(2)	0.018(2)	0.0212(6)	0.020(1)	0.021(1)	0.0347(9)	0.0329(9)	0.034(1)
U^*100 O(5)	2.6(9)	1.6(7)	3.5(3)	2.6(9)	1.1(2)	2.5(6)	2.8(6)	3.1(5)	3.1(5)	3.7(6)
x/a	0.170(2)	0.167(2)	0.171(2)	0.171(2)	0.1787(8)	0.173(1)	0.176(1)	0.162(1)	0.162(1)	0.162(1)
y/b	0.036(3)	0.043(3)	0.046(3)	0.038(3)	0.035(1)	0.042(2)	0.039(2)	0.014(2)	0.013(1)	0.016(2)
z/c	0.188(2)	0.187(2)	0.193(2)	0.190(2)	0.1895(7)	0.190(1)	0.187(1)	0.2239(9)	0.2250(8)	0.224(1)
U^*100 O(6)	4.0(9)	3.3(8)	3.5(3)	5.1(9)	2.1(3)	4.4(6)	1.7(5)	2.3(4)	2.2(4)	2.4(5)
x/a	0.304(1)	0.305(1)	0.330(2)	0.295(2)	0.2939(6)	0.291(1)	0.2942(9)	0.2545(8)	0.2518(8)	0.2533(9)
y/b	0.370(4)	0.371(5)	0.364(7)	0.358(5)	0.380(2)	0.369(4)	0.375(3)	0.364(2)	0.358(2)	0.357(2)
z/c	0.169(1)	0.175(1)	0.190(2)	0.169(2)	0.1659(5)	0.169(1)	0.1645(9)	0.1303(8)	0.1296(8)	0.129(1)
U^*100 O(7)	1.4(5)	1.6(8)	3.5(3)	2.3(8)	1.8(2)	3.0(5)	2.2(5)	3.1(4)	3.8(4)	4.6(4)
x/a	0.321(2)	0.318(2)	0.310(2)	0.323(2)	0.3215(8)	0.318(1)	0.324(2)	0.330(1)	0.3297(9)	0.332(1)
y/b	0.209(3)	0.216(3)	0.224(4)	0.210(3)	0.208(1)	0.214(2)	0.214(3)	0.210(1)	0.211(1)	0.211(2)
z/c	0.321(2)	0.319(2)	0.318(2)	0.316(2)	0.3139(7)	0.314(1)	0.306(1)	0.2824(9)	0.2806(9)	0.278(1)
U^*100 O(8)	2.6(9)	2.3(8)	3.5(3)	2.8(9)	2.6(3)	2.8(6)	4.1(8)	2.7(5)	2.9(5)	5.1(6)
x/a	0.337(1)	0.346(2)	0.363(2)	0.344(2)	0.3404(8)	0.346(1)	0.342(1)	0.3345(9)	0.3335(8)	0.334(1)
y/b	0.100(3)	0.091(3)	0.096(4)	0.099(3)	0.106(1)	0.098(2)	0.094(2)	0.172(2)	0.173(2)	0.172(2)
z/c	0.485(1)	0.491(1)	0.497(2)	0.489(1)	0.4867(6)	0.4864(9)	0.4856(9)	0.4717(9)	0.4715(8)	0.471(1)
U^*100 O(9)	1.4(6)	1.7(8)	3.5(3)	1.2(9)	2.5(3)	2.8(6)	2.1(5)	1.4(4)	1.4(4)	2.3(5)
x/a	0.515(2)	0.507(2)	0.499(2)	0.511(3)	0.510(1)	0.508(2)	0.512(1)	0.5160(8)	0.5159(8)	0.5159(9)
y/b	0.069(3)	0.078(3)	0.086(4)	0.065(3)	0.066(1)	0.068(2)	0.069(2)	0.047(1)	0.044(1)	0.045(1)
z/c	0.133(1)	0.132(1)	0.129(2)	0.138(1)	0.1318(8)	0.134(1)	0.1319(9)	0.1269(8)	0.1280(8)	0.1290(9)
U^*100	2.3(9)	1.8(9)	3.5(3)	2.2(9)	4.1(4)	4.7(6)	2.9(6)	1.8(4)	1.2(4)	1.3(4)

be described as bands running parallel to [0 1 0] in a zig-zag-like manner (Fig. 5). Here, up pointed (gray) and down pointed (white) rings in the band are related by the twofold screw axis and the neighboring band of the same layer is reversed. Several specific distances have been calculated (Table 4, Fig. 5) to show the transformation of the structure from Y, Eu–Er to Tm–Lu. The corresponding specific distances defined for $\text{Ca}_3\text{Y}_2(\text{Si}_3\text{O}_9)_2$ [17] are given in Table 4. The distances A, between up pointed (gray) and down pointed (white) rings in the band, C, between bands, and D, between layers, continuously decrease with the crystal radius of the rare earth ion and have a step between Er and Tm, while the distance B between ring edges of the neighboring bands increases until Er to Tm transition and then drops to Lu. Note that the distance D in Tm–Lu compounds is even less than in $\text{Ca}_3\text{Y}_2(\text{Si}_3\text{O}_9)_2$. The bands are tilted with respect to the plane of the rings. The opposite rings entering into the band and their conformation lead to a significant elongation of the bands and to an increase of the b axis after MPT.

The interatomic distances between Si and bridging O atoms are from 1.59 Å to 1.74 Å (average 1.66 Å), i.e. larger than the standard Si–O bond length, 1.60 Å, but comparable with the values reported for $\text{Ca}_3\text{Y}_2(\text{Si}_3\text{O}_9)_2$ (average 1.650 Å) [17], $\alpha\text{-CaSiO}_3$ (average 1.664 Å) [52], and $\text{BaTiSi}_3\text{O}_9$ (average 1.639 Å) [59]. The significant deviations of the Si–O distances and bond angles (Table 4) arise from different coordinations of oxygen atoms. All bridging O atoms are surrounded by one Sr/R and two Si atoms, except O(2) which is coordinated only by two Si atoms after transition. Unshared O(3), O(4) and O(8) atoms on one side of the $[\text{Si}_3\text{O}_9]$ rings are surrounded by one Si and three Sr/R atoms, i.e. total fourfold coordination (average 1.65 Å). The oxygen atoms

on the other side, O(1), O(6) and O(9), are coordinated by two Sr/R atoms and one Si atom (total threefold coordination), except O(6) which is coordinated by three Sr/R atoms and one Si atom after transition (total fourfold coordination). The average Si–O distance for all these atoms is 1.53 Å. Note that X-ray powder diffraction data are not the best base for accurate determination of oxygen atomic coordinates. So, Si–O bond distances sometimes deviate from the expected value 1.6 Å and the standard deviations are large, nevertheless, the mean values follow well the tendencies occurring in silicates.

Three independent Sr/R sites are coordinated by eight, seven and six oxygen atoms of $[\text{Si}_3\text{O}_9]$. The strontium and rare earth populations have been found to change from mixed to partly ordered populations as a result of MPT (Table 2). The populations of Sr^{2+} and R^{3+} in the Sr(1)/R(1) site are 0.6–0.7/0.4–0.3 before the transition and 0.5/0.5 in three standard deviations after the transition. This site is surrounded by eight O atoms, but the conformation and mutual shifts of the rings in the structure lead to the changes in the first and second coordination spheres, so that bridging O(2) atom moves from bonded to non-bonded distance, while bridging O(5) atom moves in the opposite direction (Fig. 6). The Sr(1)/R(1)–O distance is 2.59–2.64 Å and after the transition it decreases to 2.51–2.52 Å, that is consistent with an increase in the R^{3+} fraction. In the Sr(2)/R(2) site, the strontium fraction gradually increases from 0.699 to 0.75 and after the transition it steps up to 1.0, i.e. full occupation by strontium. Seven oxygen atoms surround this site. Bridging O(5) atom moves from bonded to non-bonded distance after the transition, while apical O(6) atom moves in the opposite

Table 3Selected interatomic distances (d) in $\text{Sr}_3\text{R}_2(\text{Si}_3\text{O}_9)_2$, R=Y, Eu–Lu.

Bond d , Å	Eu	Gd	Tb	Dy	Y	Ho	Er	Tm	Yb	Lu
Sr(1)/R(1)–O(1)	2.45(2)	2.56(3)	2.61(3)	2.41(5)	2.41(1)	2.42(2)	2.35(2)	2.37(1)	2.35(1)	2.38(2)
Sr(1)/R(1)–O(2)	2.85(2)	2.87(2)	3.08(2)	2.98(2)	2.924(9)	2.96(1)	2.94(1)	3.40(1)	3.410(9)	3.43(1)
Sr(1)/R(1)–O(3)	2.62(3)	2.67(3)	2.82(4)	2.59(3)	2.639(9)	2.66(2)	2.62(2)	2.44(1)	2.42(1)	2.45(2)
Sr(1)/R(1)–O(4)	2.43(3)	2.41(2)	2.30(4)	2.36(3)	2.40(1)	2.41(2)	2.38(2)	2.38(1)	2.37(1)	2.36(2)
Sr(1)/R(1)–O(5)	3.44(2)	3.43(2)	3.32(3)	3.36(3)	3.39(1)	3.35(2)	3.41(2)	2.67(1)	2.67(1)	2.67(1)
Sr(1)/R(1)–O(6)	2.42(3)	2.46(4)	2.57(4)	2.50(4)	2.33(1)	2.43(2)	2.35(2)	2.46(2)	2.52(1)	2.52(2)
Sr(1)/R(1)–O(7)	2.66(2)	2.66(2)	2.58(3)	2.68(3)	2.72(1)	2.67(2)	2.80(2)	2.96(1)	2.97(1)	3.02(2)
Sr(1)/R(1)–O(8)	2.66(2)	2.81(2)	3.02(3)	2.73(3)	2.67(1)	2.74(2)	2.67(2)	2.41(1)	2.40(1)	2.39(1)
Sr(1)/R(1)–O(8)	2.70(2)	2.71(2)	2.65(3)	2.68(2)	2.65(1)	2.71(2)	2.73(2)	2.37(1)	2.35(1)	2.35(1)
Sr(1)/R(1)–O	2.60	2.64	2.70	2.62	2.59	2.62	2.60	2.51	2.51	2.52
Sr(2)/R(2)–O(3)	2.77(2)	2.70(3)	2.56(4)	2.78(3)	2.66(1)	2.68(2)	2.70(2)	3.00(1)	2.97(1)	2.95(2)
Sr(2)/R(2)–O(4)	2.49(2)	2.45(2)	2.59(3)	2.65(3)	2.598(9)	2.62(2)	2.61(2)	2.58(1)	2.59(1)	2.59(1)
Sr(2)/R(2)–O(4)	2.65(3)	2.63(3)	2.58(3)	2.61(3)	2.621(9)	2.58(2)	2.62(2)	2.70(1)	2.68(1)	2.68(2)
Sr(2)/R(2)–O(5)	2.93(2)	2.91(2)	2.86(3)	2.93(3)	2.84(1)	2.91(2)	2.86(1)	3.73(1)	3.71(J)	3.69(2)
Sr(2)/R(2)–O(6)	2.39(3)	2.45(4)	2.52(4)	2.36(3)	2.48(1)	2.45(2)	2.45(2)	2.61(1)	2.58(1)	2.55(1)
Sr(2)/R(2)–O(6)	4.21(3)	4.29(4)	4.60(5)	4.09(3)	4.06(1)	4.05(3)	4.00(2)	2.71(1)	2.69(1)	2.70(1)
Sr(2)/R(2)–O(8)	2.33(2)	2.21(2)	2.18(3)	2.25(2)	2.30(1)	2.25(2)	2.22(2)	2.69(1)	2.71(1)	2.71(2)
Sr(2)/R(2)–O(9)	2.57(2)	2.45(2)	2.36(3)	2.54(4)	2.46(1)	2.47(2)	2.48(2)	2.55(1)	2.55(1)	2.54(1)
Sr(2)/R(2)–O	2.59	2.54	2.52	2.59	2.57	2.56	2.56	2.69	2.68	2.68
Sr(3)/R(3)–O(1)	$2 \times 2.40(2)$	$2 \times 2.32(2)$	$2 \times 2.22(3)$	$2 \times 2.36(3)$	$2 \times 2.32(1)$	$2 \times 2.30(2)$	$2 \times 2.35(2)$	$2 \times 2.33(2)$	$2 \times 2.35(2)$	$2 \times 2.32(2)$
Sr(3)/R(3)–O(3)	$2 \times 2.30(2)$	$2 \times 2.30(2)$	$2 \times 2.34(3)$	$2 \times 2.21(2)$	$2 \times 2.264(7)$	$2 \times 2.23(1)$	$2 \times 2.19(1)$	$2 \times 2.24(1)$	$2 \times 2.24(1)$	$2 \times 2.21(1)$
Sr(3)/R(3)–O(9)	$2 \times 2.33(2)$	$2 \times 2.38(2)$	$2 \times 2.47(3)$	$2 \times 2.24(2)$	$2 \times 2.31(1)$	$2 \times 2.30(2)$	$2 \times 2.33(2)$	$2 \times 2.23(1)$	$2 \times 2.21(1)$	$2 \times 2.21(1)$
Sr(3)/R(3)–O	2.34	2.33	2.34	2.27	2.30	2.27	2.29	2.27	2.27	2.24
Si(1)–O	1.58	1.58	1.55	1.60	1.63	1.60	1.61	1.61	1.60	1.61
Si(2)–O	1.62	1.59	1.55	1.62	1.60	1.60	1.61	1.62	1.62	1.63
Si(3)–O	1.67	1.68	1.76	1.65	1.64	1.66	1.66	1.64	1.65	1.63
Si(1)–Si(2)	3.00(2)	3.04(2)	2.96(2)	3.01(2)	3.03(1)	3.01(1)	3.02(1)	2.94(1)	2.935(9)	2.94(1)
Si(1)–Si(3)	3.09(2)	3.12(2)	3.18(2)	3.02(1)	3.089(8)	3.044(8)	3.051(8)	2.922(7)	2.917(7)	2.908(8)
Si(2)–Si(3)	3.13(2)	3.12(2)	3.26	3.07(2)	3.12(1))	3.06(1)	3.06(1)	2.99(1)	2.98(1)	2.98(1)
Si–Si	3.08	3.09	3.13	3.03	3.08	3.04	3.04	2.95	2.944	2.94

Distances to the second coordination sphere are denoted in italics, average distances are given in bold.

direction. The Sr(2)/R(2)–O distance is 2.54–2.59 Å and after the transition it increases to 2.68–2.69 Å, that is in general agreement with the growing strontium fraction. The value of the rare earth fraction in the Sr(3)/R(3) site is 0.74–0.79 and after the transition it steps up to 1.0 in three standard deviations, i.e. full occupation by R^{3+} . This site is coordinated by six O atoms. The surrounding oxygen atoms do not change at the transition. The Sr(3)/R(3)–O distance slightly decreases from 2.34 Å to 2.24 Å.

Following the conclusion made by V.M. Goldschmidt about the close relation between isomorphism, polymorphism and morphotropy, a polymorphic phase transition can be predicted for this series [60]. The idea is based on the dependence of effective sizes of structural units or crystal radii on external factors, such as temperature and pressure. Pressure decreases the size of structure units and should induce a structure transition (1)→(2), while temperature increases the size and should cause a polymorphic transition (2)→(1).

P→

Eu–Er (1)↔Tm–Lu (2)

←T

As soon as the difference in the crystal radii of these rare earth elements is not significant, 1.001 Å–1.087 Å, one can expect easy transitions caused by temperature and pressure. In other words, the examined materials could be phosphors sensitive to these factors. However, this prediction needs to be confirmed by further experimental work.

3.2. Luminescence properties

A linear dependence between the unit cell parameters and volume in the whole range of x has been observed for the solid

solution $\text{Sr}_3\text{Y}_{2-x}\text{Eu}_x(\text{Si}_3\text{O}_9)_2$, $x=0.25$ –2 (Fig. 7). Fig. 8 shows the room temperature excitation and emission spectra of the $\text{Sr}_3\text{Y}_{1.5}\text{Eu}_{0.5}(\text{Si}_3\text{O}_9)_2$ powder. The spectra contain a large band in the UV and characteristic lines in the visible spectral range that correspond to the Eu^{3+} 4f–4f transitions. The wide band located at ~233 nm (5.3 eV) in the excitation spectra is a charge transfer band (CTB), corresponding to an electron transfer from an oxygen 2p orbital to an empty 4f orbital of europium (Fig. 8a). The position of CTB is close to that in other silicates, e.g. $\beta\text{-Y}_2\text{Si}_2\text{O}_7$ (5.56 eV) and $\text{Na}_3\text{YSi}_3\text{O}_9$ (5.56 eV) [61]. The charge transfer energy is known to decrease with larger average distance to the surrounding anions [62–64]. The interatomic distance $\langle \text{Y–O} \rangle$ equals 2.26 Å in $\beta\text{-Y}_2\text{Si}_2\text{O}_7$ (S.G. C2/m) and europium substitutes for yttrium ions in YO_6 octahedra [65], while the average distances $\langle \text{Y–O} \rangle$ vary between 2.30 Å and 2.59 Å (Table 3) and Y^{3+} ions share 6-, 7- and 8-fold coordination symmetry sites in $\text{Sr}_3\text{Y}_2(\text{Si}_3\text{O}_9)_2$. Therefore, the CTB extends to longer wavelengths in the $\text{Sr}_3\text{Y}_2(\text{Si}_3\text{O}_9)_2$ cyclosilicate than in the $\beta\text{-Y}_2\text{Si}_2\text{O}_7$ pyrosilicate.

The dependence of the $\text{Sr}_3\text{Y}_{2-x}\text{Eu}_x(\text{Si}_3\text{O}_9)_2$ integrated emission intensity, upon excitation at 233 nm, on the europium doping concentration is shown in Fig. 8b (lower inset). The PL intensity increases with Eu^{3+} concentration until the emission intensity maximum is reached. The strongest emission signal is attained in the solid solution $\text{Sr}_3\text{Y}_{2-x}\text{Eu}_x(\text{Si}_3\text{O}_9)_2$, where $x=0.5$, i.e. with 25 mol.% europium content. Similar values of Eu^{3+} optimal concentration in some silicates and oxyapatites have been discussed elsewhere [4,66]. When the Eu^{3+} concentration exceeds 25 mol.%, the emission intensity decreases due to concentration quenching which is less pronounced. The arrangement of the lanthanide ions in three non-equivalent sites in the layered structure of the $\text{Sr}_3\text{Y}_2(\text{Si}_3\text{O}_9)_2$ host reduces their ability to interact,

Table 4Bond angles (ω) and specific distances in $\text{Sr}_3\text{R}_2(\text{Si}_3\text{O}_9)_2$, R=Y, Eu–Lu.

Angle ω , °	Eu	Gd	Tb	Dy	Y	Ho	Er	Tm	Yb	Lu
O(1)-Si(1)-O(2)	108.0 (14)	114.8 (16)	105.6 (16)	108.3 (20)	106.5 (7)	109.8 (10)	104.6 (10)	107.0 (9)	105.7 (8)	108.1 (9)
O(1)-Si(1)-O(4)	123.0 (14)	125.1 (15)	123.9 (19)	120.3 (17)	121.3 (6)	120.7 (10)	122.3 (10)	114.4 (8)	113.3 (8)	113.6 (9)
O(1)-Si(1)-O(5)	114.5 (15)	108.9 (17)	108.4 (18)	110.3 (19)	115.4 (7)	109.7 (10)	116.5 (10)	114.8 (8)	115.7 (8)	112.3 (9)
O(2)-Si(1)-O(4)	96.1 (13)	96.8 (13)	97.6 (18)	101.0 (17)	99.4 (6)	102.2 (10)	98.7 (10)	109.4 (8)	110.2 (7)	112.8 (8)
O(2)-Si(1)-O(5)	108.6 (12)	105.7 (13)	104.6 (16)	106.7 (15)	105.6 (5)	106.2 (9)	106.3 (8)	103.5 (7)	102.5 (7)	102.0 (7)
O(4)-Si(1)-O(5)	104.5 (12)	103.6 (14)	113.9 (15)	109.2 (17)	106.3 (6)	107.2 (9)	105.8 (8)	107.0 (8)	108.7 (7)	107.4 (9)
O-Si(1)-O	109.1	109.2	109.0	109.3	109.1	109.3	109.0	109.4	109.4	109.4
O(3)-Si(2)-O(5)	108.5 (16)	106.2 (17)	105.6 (25)	110.0 (18)	100.7 (7)	105.3 (11)	104.0 (9)	114.4 (8)	114.0 (8)	113.0 (9)
O(3)-Si(2)-O(6)	123.1 (10)	125.5 (12)	146.2 (24)	119.5 (12)	123.2 (6)	119.4 (8)	121.9 (8)	117.2 (6)	116.8 (6)	117.5 (7)
O(3)-Si(2)-O(7)	105.2 (13)	104.1 (15)	100.1 (21)	105.6 (16)	103.8 (7)	102.7 (10)	108.3 (11)	107.3 (9)	108.3 (8)	111.0 (10)
O(5)-Si(2)-O(6)	104.2 (16)	105.0 (21)	99.5 (25)	109.3 (21)	107.9 (10)	111.9 (14)	108.5 (13)	106.5 (9)	107.2 (9)	107.0 (10)
O(5)-Si(2)-O(7)	104.1 (9)	103.0 (10)	104.5 (13)	104.3 (10)	104.4 (5)	105.9 (6)	105.0 (7)	103.1 (6)	102.9 (6)	102.5 (7)
O(6)-Si(2)-O(7)	110.3 (18)	110.9 (23)	95.0 (26)	106.9 (22)	114.6 (9)	110.4 (14)	107.8 (13)	107.3 (9)	106.5 (8)	104.5 (10)
O-Si(2)-O	109.2	109.1	108.5	109.3	109.1	109.3	109.3	109.3	109.3	109.3
O(2)-Si(3)-O(7)	100.5 (11)	98.3 (13)	89.5 (13)	102.0 (14)	103.2 (6)	102.6 (8)	103.8 (9)	102.6 (6)	101.4 (6)	100.1 (7)
O(2)-Si(3)-O(8)	114.8 (12)	112.9 (12)	114.4 (14)	114.9 (15)	110.6 (6)	111.5 (8)	113.1 (9)	109.5 (6)	109.6 (6)	109.8 (7)
O(2)-Si(3)-O(9)	114.2 (12)	110.3 (13)	109.1 (15)	108.8 (17)	110.5 (7)	109.5 (10)	111.0 (10)	110.6 (7)	111.8 (7)	111.2 (8)
O(7)-Si(3)-O(8)	102.0 (11)	107.4 (12)	110.7 (14)	109.3 (14)	105.2 (6)	107.5 (8)	108.8 (9)	104.5 (7)	103.7 (7)	104.5 (8)
O(7)-Si(3)-O(9)	107.1 (13)	114.0 (14)	121.5 (17)	108.0 (17)	112.5 (8)	115.6 (10)	111.3 (10)	113.2 (8)	112.9 (7)	113.3 (9)
O(8)-Si(3)-O(9)	115.8 (13)	113.1 (13)	110.3 (17)	113.0 (15)	114.2 (7)	110.1 (9)	108.7 (9)	115.6 (8)	116.2 (7)	116.5 (8)
O-Si(3)-O	109.1	109.3	109.3	109.4	109.5	109.5	109.3	109.3	109.3	109.2
Si(1)-O(5)-Si(2)	135.4 (16)	135.6 (17)	137.5 (19)	132.5 (18)	135.8 (7)	133.5 (11)	135.7 (10)	129.7 (8)	129.3 (8)	127.6 (9)
Si(1)-O(2)-Si(3)	133.6 (10)	137.7 (13)	141.7 (15)	133.1 (12)	132.6 (6)	133.9 (7)	131.5 (9)	124.0 (7)	124.7 (7)	125.8 (8)
Si(2)-O(7)-Si(3)	136.2 (16)	138.2 (17)	136.2 (19)	136.4 (18)	136.4 (8)	135.2 (10)	134.9 (13)	128.8 (9)	128.9 (8)	128.9 (10)
A, Å	0.811	0.785	0.675	0.745	0.670	0.727	0.673	0.417	0.408	0.390
B, Å	3.877	3.943	3.861	3.988	3.969	4.061	4.007	3.946	3.934	3.953
C, Å	10.166	10.132	10.081	10.051	10.023	10.018	9.983	9.300	9.285	9.266
D, Å	5.017	5.016	5.004	5.004	5.004	5.002	4.997	4.927	4.925	4.922

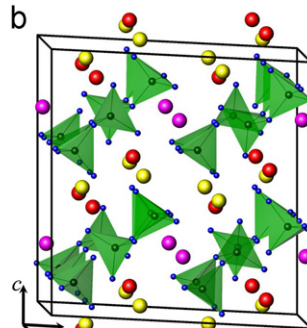
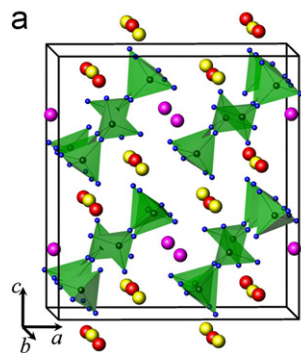
Specific distances calculated for $\text{Ca}_3\text{Y}_2(\text{Si}_3\text{O}_9)_2$ [17]: A=0.863 Å, B=3.787 Å, C=9.928 Å, D=4.959 Å.

Fig. 3. The crystal structure of $\text{Sr}_3\text{Er}_2(\text{Si}_3\text{O}_9)_2$ (a) and $\text{Sr}_3\text{Tm}_2(\text{Si}_3\text{O}_9)_2$ (b) showing the SiO_4 tetrahedra (green), $\text{Sr}(1)/\text{R}(1)$ atoms (red), $\text{Sr}(2)/\text{R}(2)$ atoms (yellow), and $\text{Sr}(3)/\text{R}(3)$ atoms (lilac). (For interpretation of the references to color in this figure caption, the reader is referred to the web version of this article.)

which in turn opens an opportunity to introduce a relatively high dopant content without emission quenching [67]. The ${}^5\text{D}_0 \rightarrow {}^7\text{F}_0$ transition is located at ~ 577 nm, ${}^5\text{D}_0 \rightarrow {}^7\text{F}_1$ at ~ 590 nm, ${}^5\text{D}_0 \rightarrow {}^7\text{F}_2$ at ~ 610 nm, ${}^5\text{D}_0 \rightarrow {}^7\text{F}_3$ at ~ 650 nm, and ${}^5\text{D}_0 \rightarrow {}^7\text{F}_4$ at ~ 702 nm.

The first line in the emission spectrum is related to the ${}^5\text{D}_0 \rightarrow {}^7\text{F}_0$ transition ($0 \leftrightarrow 0$ emission) and, according to the Judd–Ofelt theory [68], it must be forbidden owing to the transition probability from $J=0$ to $J'=0$. However, Blasse et al. reported that for low crystal symmetries such as C_s , C_n , or C_{nv} , the above-mentioned transition is partially allowed by the group theory and is often observed [69]. The Eu^{3+} ions occupy the Y^{3+} sites in distorted oxygen octahedra (C_2 local symmetry; coordination number CN=6) and oxygen polyhedra with CN=7 (C_1) and CN=8 (C_1). Thus, the ${}^5\text{D}_0 \rightarrow {}^7\text{F}_0$ radiative transition should show three peaks in the emission spectrum, which can be

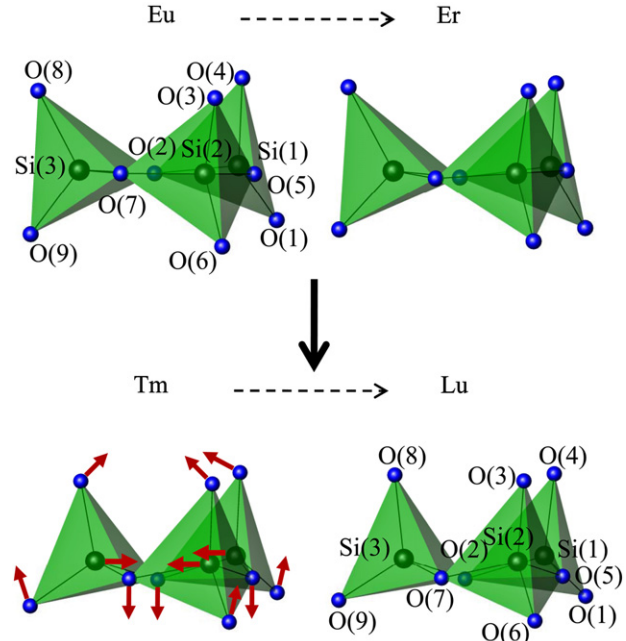


Fig. 4. The change of the $[\text{Si}_3\text{O}_9]$ ring conformation in $\text{Sr}_3\text{R}_2(\text{Si}_3\text{O}_9)_2$, R=Eu, Er, Tm and Lu.

registered usually at low temperatures [70]. In the room temperature emission spectrum, only an unresolved low intensity ${}^5\text{D}_0 \rightarrow {}^7\text{F}_0$ line can be distinguished.

The second band is associated with the ${}^5\text{D}_0 \rightarrow {}^7\text{F}_1$ magnetic dipole (MD) transition and the most intense third band is the ${}^5\text{D}_0 \rightarrow {}^7\text{F}_2$ electric dipole(ED) transition, in which the final levels are thermally populated at room temperature (Fig. 8b). The two

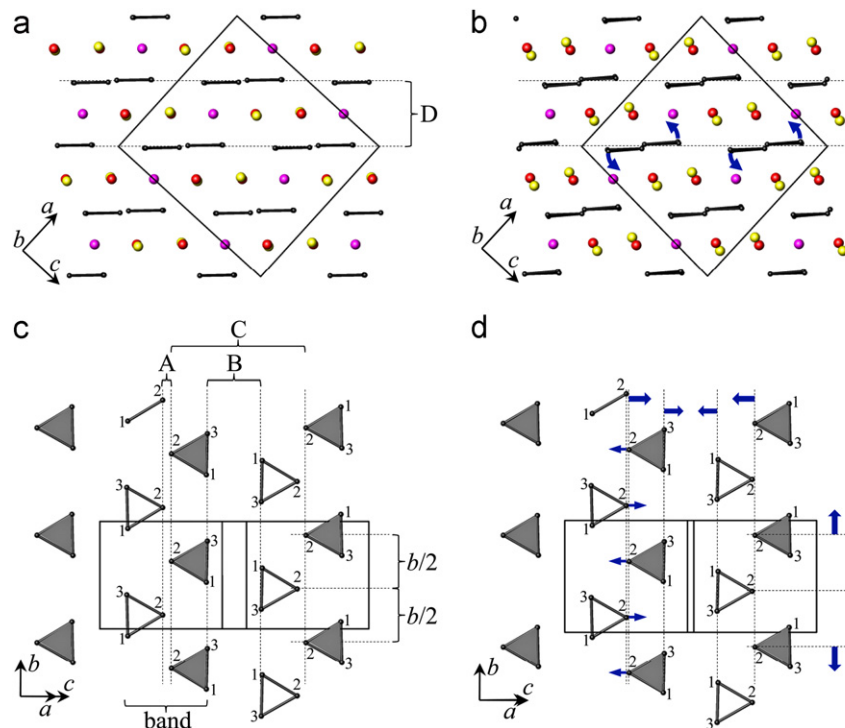


Fig. 5. Projection of the whole structure of $\text{Sr}_3\text{Er}_2(\text{Si}_3\text{O}_9)_2$ (a) and $\text{Sr}_3\text{Tm}_2(\text{Si}_3\text{O}_9)_2$ (b) parallel to $[0\ 1\ 0]$. Single layer containing $[\text{Si}_3\text{O}_9]$ rings arranged in bands (up pointed (grey) and down pointed (white)) of $\text{Sr}_3\text{Er}_2(\text{Si}_3\text{O}_9)_2$ (c) and $\text{Sr}_3\text{Tm}_2(\text{Si}_3\text{O}_9)_2$ (d). Oxygen atoms are omitted for clear reading.

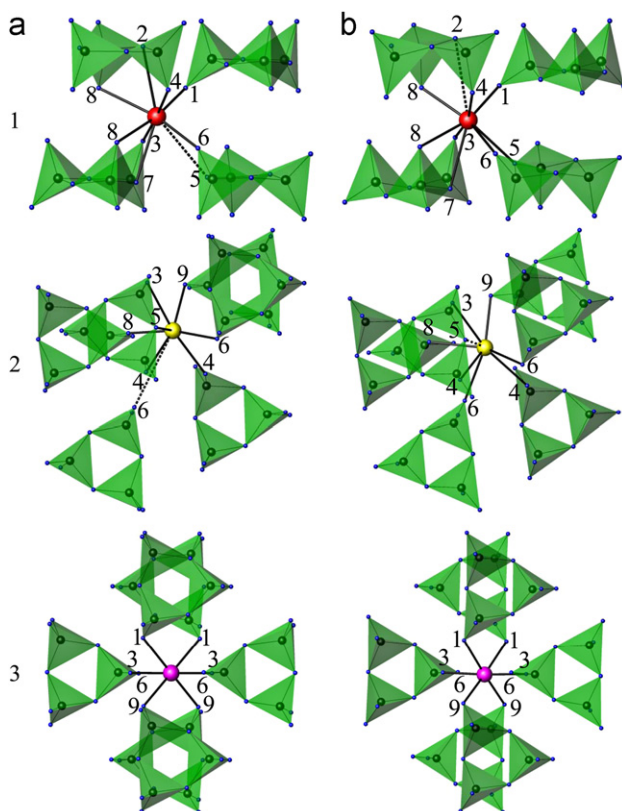


Fig. 6. Coordination environment of the three non-equivalent cations within the structure of $\text{Sr}_3\text{Er}_2(\text{Si}_3\text{O}_9)_2$ (a) and $\text{Sr}_3\text{Tm}_2(\text{Si}_3\text{O}_9)_2$ (b): 1— $\text{Sr}(1)/\text{R}(1)$, 2— $\text{Sr}(2)/\text{R}(2)$, 3— $\text{Sr}(3)/\text{R}(3)$. Solid and dashed lines show distances in the first and second coordination spheres, respectively.

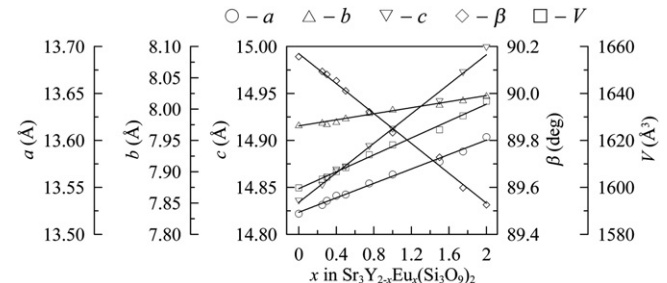


Fig. 7. Variation of the unit cell constants for $\text{Sr}_3\text{Y}_{2-x}\text{Eu}_x(\text{Si}_3\text{O}_9)_2$, $x=0-2$.

other bands of lower intensity are associated with $^5\text{D}_0 \rightarrow ^7\text{F}_3$ and $^5\text{D}_0 \rightarrow ^7\text{F}_4$ transitions, respectively. The hypersensitive ED transition ($^5\text{D}_0 \rightarrow ^7\text{F}_2$) can occur only in non-centrosymmetric systems [68] that agrees with the expected C_1 and C_2 site symmetries of the Eu^{3+} ions in $\text{Sr}_3\text{Y}_2(\text{Si}_3\text{O}_9)_2$. The well-known asymmetry ratio of integrated intensities of the $^5\text{D}_0 \rightarrow ^7\text{F}_2$ (ED) and $^5\text{D}_0 \rightarrow ^7\text{F}_1$ (MD) transitions can be considered indicative of the asymmetry of the coordination polyhedron of the Eu^{3+} ion. It is a good measure for the symmetry of the Eu^{3+} site and can be used as an indicator for the relative magnitude of hypersensitivity (Eq. (1))

$$R = \frac{I(^5\text{D}_0 \rightarrow ^7\text{F}_2)}{I(^5\text{D}_0 \rightarrow ^7\text{F}_1)} \quad (1)$$

In a sense, the higher is the I_{0-2}/I_{0-1} ratio, the more apart from a centrosymmetric geometry Eu^{3+} is located. High values of R indicate that there is both an enhancement of the electric dipole transition and an increase in the crystal field strength that could be related to an increase in the covalence or to the distortion of the bonds surrounding the active ion. The calculated values of R

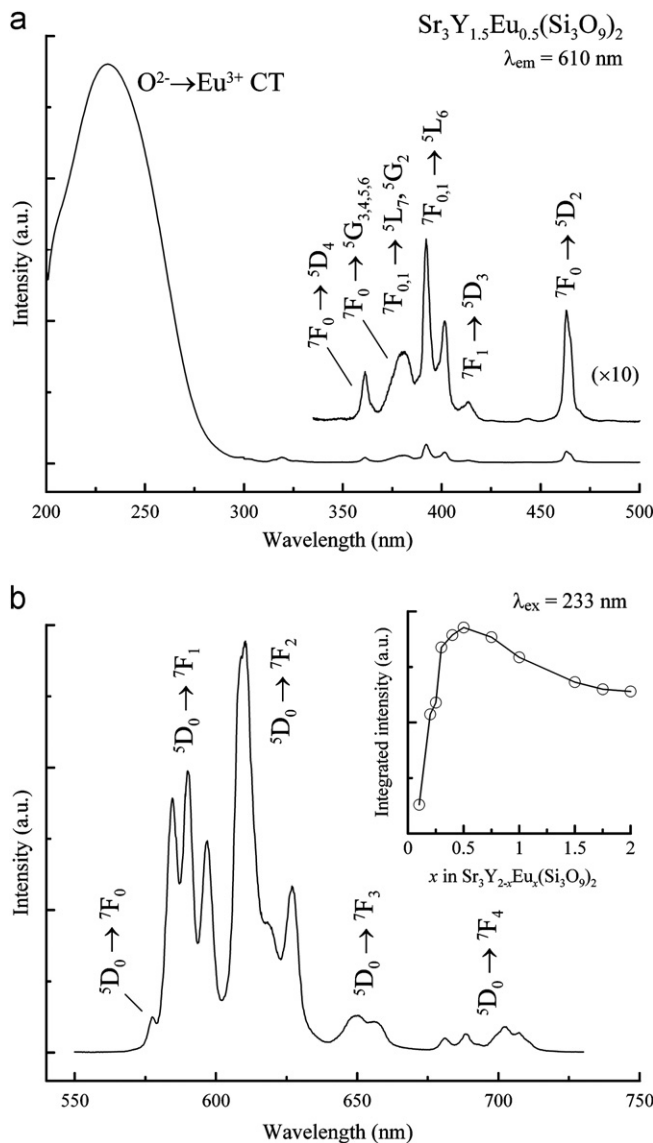


Fig. 8. The room temperature excitation spectrum of $\text{Sr}_3\text{Y}_{1.5}\text{Eu}_{0.5}(\text{Si}_3\text{O}_9)_2$ upon monitoring emission at 610 nm (a) and emission spectrum excited at 233 nm (b). The enlarged part of the excitation spectrum (330–500 nm) is plotted in the upper inset. The lower inset shows the effect of Eu^{3+} concentration on the integrated PL intensity for the $\text{Sr}_3\text{Y}_{2-x}\text{Eu}_x(\text{Si}_3\text{O}_9)_2$, $x=0.25\text{--}2$, powders.

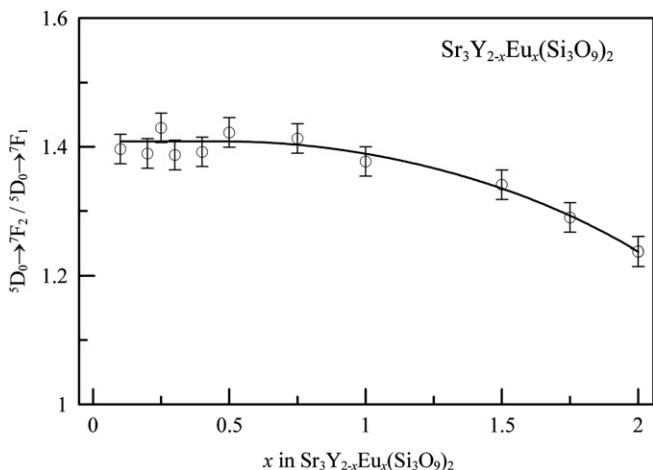


Fig. 9. The dependence of asymmetry parameter R on the europium doping concentration (x) in $\text{Sr}_3\text{Y}_{2-x}\text{Eu}_x(\text{Si}_3\text{O}_9)_2$.

as function of the Eu^{3+} concentration are presented in Fig. 9. One can note that the R parameter slightly decreases with increasing the Eu^{3+} content. Therefore, it can be concluded that the local symmetry of Eu^{3+} increases when x tends to the limit 2 in the $\text{Sr}_3\text{Y}_{2-x}\text{Eu}_x(\text{Si}_3\text{O}_9)_2$ solid solution. The obtained values of I_{0-2}/I_{0-1} descending from 1.43 to 1.24 for the emission spectra of $\text{Sr}_3\text{Y}_2(\text{Si}_3\text{O}_9)_2:\text{Eu}^{3+}$ are comparable with those for $\text{CaSiO}_3:\text{Eu}^{3+}$ [71].

4. Conclusions

The series of promising luminescent materials, cyclosilicates $\text{Sr}_3\text{R}_2(\text{Si}_3\text{O}_9)_2$, $\text{R}=\text{Y}, \text{Eu-Lu}$, has been synthesized for the first time. X-ray and neutron powder diffraction studies show that these oxides crystallize in the monoclinic crystal system (S.G. C2/c, $Z=4$) and have a morphotropic phase transition between Er and Tm compounds followed by a step-like change of the unit cell constants. Isolated $[\text{Si}_3\text{O}_9]$ rings are located in layers stacking with Sr/R layers along the $[1\ 0\ \bar{1}]$ direction. The rare earth atoms are distributed among three independent Sr/R sites coordinated by 8, 7 and 6 oxygen atoms, respectively.

As a result of the transition: (a) the Sr-R populations change from mixed to 0.5/0.5 over site (1) and full occupation of sites (2) and (3) by Sr and R, respectively; (b) the conformation of $[\text{Si}_3\text{O}_9]$ rings changes from nearly ideal to point up boat conformation, (c) the Si-Si distances decrease from 3.03–3.08 Å to 2.94–2.95 Å; (d) oxygen atoms exchange from the first and the second coordination sphere of two Sr/R sites; and (e) this structure transformation could be induced by variation of temperature and pressure.

$\text{Sr}_3\text{Y}_2(\text{Si}_3\text{O}_9)_2:\text{Eu}^{3+}$ under UV excitation shows luminescence in the visible spectral region owing to intra-configurational 4f-4f transitions in trivalent europium ions. From the analysis of the obtained emission spectra, the best dopant concentrations have been established to be 25 mol.% for $\text{Sr}_3\text{Y}_2(\text{Si}_3\text{O}_9)_2$. These compounds demonstrate multiband photoluminescence emission in the orange-red spectral region, which is useful for generating white light.

Supporting information

Crystallographic information file (CIF) of $\text{Sr}_3\text{R}_2(\text{Si}_3\text{O}_9)_2$, $\text{R}=\text{Y}, \text{Eu-Lu}$ contains the supplementary crystallographic data for this paper. These data can be obtained free of charge from the Cambridge Crystallographic Data Center via <http://www.ccdc.cam.ac.uk/conts/retrieving.html>.

Acknowledgments

Authors thank Dr. A. Garcia (ICMAB-CNRS, Pessac, France) for fruitful discussions. This work was supported by the UB RAS under Grants nos. 12-T-3-1009, 10-3-02 and 11-3-01.

Appendix A. Supporting information

Supplementary data associated with this article can be found in the online version at <http://dx.doi.org/10.1016/j.jssc.2012.09.009>.

References

- [1] J. Koike, T. Kojima, R. Toyonaga, A. Kagami, T. Hase, S. Inaho, J. Electrochem. Soc. 126 (1979) 1008–1010.
- [2] B. Yan, L. Zhou, Mater. Res. Bull. 45 (2010) 1768–1770.

- [3] A.N. Belsky, J.C. Krupa, Displays 19 (1999) 185–196.
- [4] Z.Y. Zhang, Y.H. Wang, J.C. Zhang, Y. Hao, Mater. Res. Bull. 43 (2008) 926–931.
- [5] M.E. Fleet, X. Liu, J. Solid State Chem. 161 (2001) 166–172.
- [6] F. Monteverde, G. Celotti, J. Eur. Ceram. Soc. 22 (2002) 721–730.
- [7] B. Howe, A.L. Diaz, J. Lumin. 109 (2004) 51–59.
- [8] K.I. Machida, G.Y. Adachi, J. Shiokawa, M. Shimada, M. Koizumi, K. Suito, A. Onodera, Inorg. Chem. 21 (1982) 1512–1519.
- [9] S.H.M. Poort, H.M. Reijnhoudt, H.G.T. van der Kuip, G. Blasse, J. Alloys Compd. 241 (1996) 75–81, and references therein.
- [10] S.H.M. Poort, A. Meijerink, G. Blasse, J. Phys. Chem. Solids 58 (1997) 1451–1456.
- [11] Z.G. Cui, G.H. Jia, D.G. Deng, Y.J. Hua, S.L. Zhao, L.H. Huang, H.P. Wang, H.P. Ma, S.Q. Xu, J. Lumin. 132 (2012) 153–160.
- [12] G. Engel, K. Cee, Z. Anorg. Allg. Chem. 621 (1995) 1803–1807.
- [13] H. Yamane, T. Nagasawa, M. Shimada, T. Endo, Acta Crystallogr. C 53 (1997) 1367–1369.
- [14] H. Yamane, T. Nagasawa, Y. Murakami, T. Kamata, D. Shindo, M. Shimada, T. Endo, Mater. Res. Bull. 33 (1998) 845–853.
- [15] J. Ito, Am. Mineral. 53 (1968) 890–907.
- [16] W.L. Wanmaker, J.W. Vrugt, J.G. Verlijssdonk, Philips Res. Rep. 26 (1971) 373–381.
- [17] H. Yamane, T. Nagasawa, M. Shimada, T. Endo, Acta Crystallogr. C 53 (1997) 1533–1536.
- [18] T. Endo, Jpn. Patent JP 2005-048146, February 24, 2005.
- [19] D. Santamaría-Pérez, A. Vegas, F. Liebau, Struct. Bond. 118 (2005) 121–177.
- [20] B.V. Rao, Y.T. Nien, W.S. Hwang, I.G. Chen, J. Electrochem. Soc. 156 (2009) J338–J341.
- [21] F. Piccinelli, A. Speghini, G. Mariotto, L. Bovo, M. Bettinelli, J. Rare Earths 27 (2009) 555–559.
- [22] V.R. Bandi, Y.T. Nien, T.H. Lu, I.G. Chen, J. Am. Ceram. Soc. 92 (2009) 2953–2956.
- [23] K.V. Ivanovskikh, A. Meijerink, F. Piccinelli, A. Speghini, E.I. Zinin, C. Ronda, M. Bettinelli, J. Lumin. 130 (2010) 893–901.
- [24] V.R. Bandi, Y.T. Nien, I.G. Chen, J. Appl. Phys. 108 (2010) 023111.
- [25] V.R. Bandi, B.K. Grandhe, K. Jang, H.S. Lee, S.S. Yi, J.H. Jeong, Ceram. Int. 37 (2011) 2001–2005.
- [26] A. Dobrowolska, E. Zych, MRS Proc. 1342 (2011) 55–60.
- [27] Z.J. Zhang, A.C.A. Delsing, P.H.L. Notten, J.T. Zhao, H.T. Hintzen, Mater. Res. Bull. 47 (2012) 2040–2044.
- [28] J. Lin, Q.A. Su, Mater. Chem. Phys. 38 (1994) 98–101.
- [29] X.M. Han, J. Lin, H.L. Zhou, M. Yu, Y.H. Zhou, M.L. Pang, J. Phys.: Condens. Matter 16 (2004) 2745–2755.
- [30] X.M. Han, J. Lin, Z. Li, X.W. Qi, M.Y. Li, X.Q. Wang, J. Rare Earths 26 (2008) 443–445.
- [31] J. Lin, Q.A. Su, J. Mater. Chem. 5 (1995) 603–606.
- [32] J. Lin, Q.A. Su, Phys. Status Solidi B: Basic Solid State Phys. 196 (1996) 261–267.
- [33] Y. Wen, Y.H. Wang, F. Zhang, B.T. Liu, Mater. Chem. Phys. 129 (2011) 1171–1175.
- [34] G.G. Li, Y. Zhang, D.L. Geng, M.M. Shang, C. Peng, Z.Y. Cheng, J. Lin, ACS Appl. Mater. Interfaces 4 (2012) 296–305.
- [35] Y. Wen, Y.H. Wang, B.T. Liu, F. Zhang, Opt. Mater. 34 (2012) 889–892.
- [36] Y.C. Chiu, W.R. Liu, Y.T. Yeh, S.M. Jang, T.M. Chen, J. Electrochem. Soc. 156 (2009) J221–J225;
- Y.C. Chiu, W.R. Liu, Y.T. Yeh, S.M. Jang, T.M. Chen, ECS Trans. 25 (2009) 157–165.
- [37] A. Dobrowolska, E. Zych, J. Solid State Chem. 184 (2011) 1707–1714.
- [38] J.E.H. Sansom, D. Richings, P.R. Slater, Solid State Ionics 139 (2001) 205–210.
- [39] L. Leon-Reina, E.R. Losilla, M. Martinez-Lara, S. Bruque, A. Llobet, D.V. Sheptyakov, M.A.G. Aranda, J. Mater. Chem. 15 (2005) 2489–2498.
- [40] L. Leon-Reina, J.M. Porras-Vazquez, E.R. Losilla, M.A.G. Aranda, Solid State Ionics 177 (2006) 1307–1315.
- [41] Y. Masubuchi, M. Higuchi, T. Takeda, S. Kikkawa, Solid State Ionics 177 (2006) 263–268.
- [42] S. Lambert, A. Vincent, E. Bruneton, S. Beaudet-Savignat, F. Guillet, B. Minot, F. Bouree, J. Solid State Chem. 179 (2006) 2602–2608.
- [43] P.E. Kazin, M.A. Zykin, O.R. Gazizova, Yu.D. Tret'yakov, Z. Anorg. Allg. Chem. 635 (2009) 2072–2076.
- [44] M. Wierzbicka-Wieczorek, U. Kolitsch, E. Tillmanns, Eur. J. Mineral. 22 (2010) 245–258.
- [45] K.I. Machida, G.Y. Adachi, J. Shiokawa, M. Shimada, M. Koizumi, Acta Crystallogr. B 38 (1982) 386–389.
- [46] R.E. Marsh, F.H. Herbstein, Acta Crystallogr. B 39 (1983) 280–287.
- [47] F. Nishi, Acta Crystallogr. C 53 (1997) 534–536.
- [48] H. Müller-Bunz, T. Schleid, Z. Anorg. Allg. Chem. 625 (1999) 1377–1383.
- [49] H. Jacobsen, G. Meyer, W. Schipper, G. Blasse, Z. Anorg. Allg. Chem. 620 (1994) 451–456.
- [50] J.G. Wang, G.B. Li, S.J. Tian, F.H. Liao, X.P. Jing, Mater. Res. Bull. 36 (2001) 2051–2057.
- [51] V. Kahlenberg, J. Alloys Compd. 366 (2004) 132–135.
- [52] T. Yamanaka, H. Mori, Acta Crystallogr. B 37 (1981) 1010–1017.
- [53] M. O'Keeffe, B.G. Hyde, in: M. O'Keeffe, A. Navrotsky (Eds.), Structure and Bonding in Crystals, Vol. 1, Academic Press, New York, 1981, pp. 227–254.
- [54] According to MPT definition, i.e. “an abrupt change in the structure of a solid solution with variation in composition”;
J.B. Clark, J.W. Hastie, L.H.E. Kihlborg, R. Metselaar, M.M. Thackeray, Pure Appl. Chem. 66 (1994) 577–594.
- [55] B.H. Toby, J. Appl. Crystallogr. 34 (2001) 210–213;
A.C. Larson, R.B. Von Dreele, General Structure Analysis System (GSAS), Los Alamos National Laboratory Report LAUR 86-748, Los Alamos, NM, 2004.
- [56] R.D. Shannon, Acta Crystallogr. A 32 (1976) 751–767;
Y.Q. Jia, J. Solid State Chem. 95 (1991) 184–187.
- [57] V. Kahlenberg, J. Konzett, R. Kaindl, J. Solid State Chem. 180 (2007) 1934–1942.
- [58] G. Dörsam, A. Liebscher, B. Wunder, G. Franz, M. Gottschalk, Eur. J. Mineral. 21 (2009) 705–714.
- [59] K. Fischer, Z. Kristallogr. 129 (1969) 222–243.
- [60] V.M. Goldschmidt, A. Muir (Eds.), Geochemistry, Clarendon Press, Oxford, England, 1954.
- [61] P. Dorenbos, J. Lumin. 111 (2005) 89–104;
C.H. Kim, H.L. Park, S. Mho, Solid State Commun. 101 (1997) 109–113;
D. Meiss, W. Wischert, S. Kemmler-Sack, Phys. Status Solidi (A) 134 (1992) 539–546.
- [62] G. Blasse, J. Solid State Chem. 4 (1972) 52–54.
- [63] H.E. Hoefdraad, J. Solid State Chem. 15 (1975) 175–177.
- [64] V. Jubera, J.P. Chaminade, A. Garcia, F. Guillen, C. Fouassier, J. Lumin. 101 (2003) 1–10.
- [65] G.J. Redhammer, G. Roth, Acta Crystallogr. C 59 (2003) i103–i106.
- [66] Y.Q. Shen, R. Chen, F. Xiao, H.D. Sun, A. Tok, Z.L. Dong, J. Solid State Chem. 183 (2010) 3093–3099.
- [67] V.B. Mikhailik, Mater. Lett. 63 (2009) 803–805.
- [68] B.R. Judd, Phys. Rev. 127 (1962) 750–761;
G.S. Ofelt, J. Chem. Phys. 37 (1962) 511–520.
- [69] G. Blasse, A. Bril, Philips Res. Rep. 21 (1966) 368–378;
W.C. Nieuwpoort, G. Blasse, Solid State Commun. 4 (1966) 227–229.
- [70] R.A. Benhamou, A. Bessière, G. Wallez, B. Viana, M. Elaatmani, M. Daoud, A. Zegzouti, J. Solid State Chem. 182 (2009) 2319–2325.
- [71] Ž. Andrić, R. Kršmanović, M. Marinović-Cincović, T. Dramićanin, B. Šećerov, M.D. Dramićanin, Acta Phys. Pol. A 112 (2007) 969–974.